EXAMENSARBETE I GEOLOGI VID LUNDS UNIVERSITET

Berggrundsgeologi

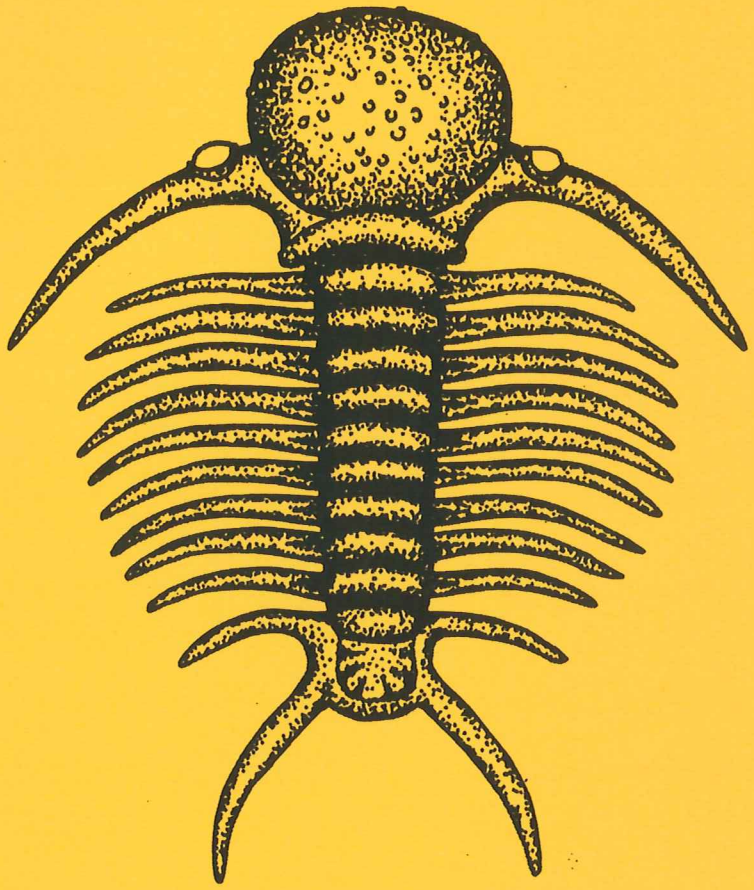

Permeability variation in a tidal Jurassic deposit, Höganäs basin, Fennoscandian Border Zone

Henrik Jonsson

Examensarbete, 20 p
Institutionen, Lunds Universitet

Nr 151

CODEN: SE-LUNBDS/NBGO-02/5151+19S

EXAMENSARBETE I GEOLOGI VID LUNDS UNIVERSITET

Berggrundsgeologi

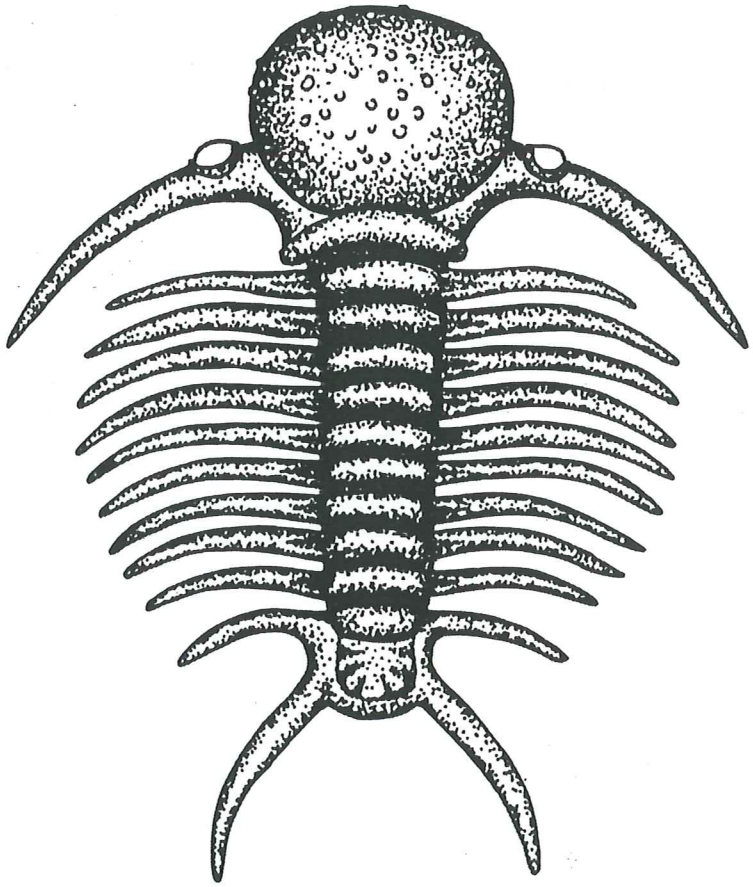

Permeability variation in a tidal Jurassic deposit, Höganäs basin, Fennoscandian Border Zone

Henrik Jonsson

Lund 2002 **Examensarbete, 20 p** **Nr 151**
Geologiska Institutionen, Lunds Universitet

Permeability variation in a tidal Jurassic deposit, Höganäs basin, Fennoscandian Border Zone

HENRIK JONSSON

Jonsson, H., 2002: Permeability variation in a tidal Jurassic deposit, Höganäs basin, Fennoscandian Border Zone. *Examensarbete i geologi vid Lunds Universitet, Berggrundsgeologiska avdelningen Nr 151*, pp. 1-19.

An examination of permeability differences was made on plugs obtained from six drill cores in both horizontal and vertical directions, representing different facies of the Hettangian strata from the Höganäs Formation. The permeability analyses distinguish permeability differences from anisotropy and an index was created to evaluate the anisotropy. The cause of the measured anisotropy in this study is a direct function of the depositional effects, related to tide-dominated deltaic environment. All thirty-eight permeability and porosity data were obtained from plugs taken from a drill core succession with a total length of thirty metres. BSE point-counting was used to obtain correct mineralogical results. The technique was particular convenient for the fine-grained sandstones. The relationship between anisotropy and depositional and diagenetic history is interpreted and a diagenetic model is proposed. Quartz cement occurs abundantly in some sandstone beds and scarcely in other similar strata, which suggests that the fluid flow in the strata was the controlling factor of the diagenetic processes.

Jurassic heterolithic sandstone reservoirs are economically important for the oil industry and the anisotropy provide sealing conditions for the reservoirs and prevents oil migration, which have an inhibiting effect on exploitation. It is suggested that prediction (modelling) of reservoir qualities needs to evaluate the importance of petrographic and petrophysical properties.

Keywords: permeability, Höganäs Formation, anisotropy, heteroliths, Lower Jurassic, quartz cement

Henrik Jonsson, Department of Geology, Sölvegatan 13, SE-223 62 Lund, Sweden. E-mail: Henrik.Jonsson@novell.geol.lu.se

Filborna waste dump (Nordvästra Skånes Renhållning, NSR) is situated a few kilometres east of the city of Helsingborg, in the north-western part of Skåne (Fig 1). In 1997 NSR carried out a drilling project to examine the groundwater table and the direction of groundwater flow under the waste dump. Forty wells were drilled down to various depths (5-40 m) and at least twenty cores were obtained, six of which penetrated Jurassic siliciclastic strata of the Helsingborg Member in the Höganäs Formation (cf. Troedsson 1950; Vossmerbäumer 1970; and Ahlberg 1994). The Höganäs Formation consists of three members that represent the sedimentary succession around the Triassic-Jurassic boundary in north-west of Skåne. The lowermost units of the Höganäs Formation, the Vallåkra and the Bjuv Members are of Rhaetian age, whereas the uppermost unit of the Höganäs Formation is the Hettangian Helsingborg Member (Fig 2). Skåne is situated at the Fennoscandian Border Zone and during the Hettangian, Skåne was located at 43°N (personal communication; T. Torsvik, Trondheim, 2001) where it was affected by tectonic activity along the Sorgenfrei-Tornquist Zone (Fig 1; Fig 3).

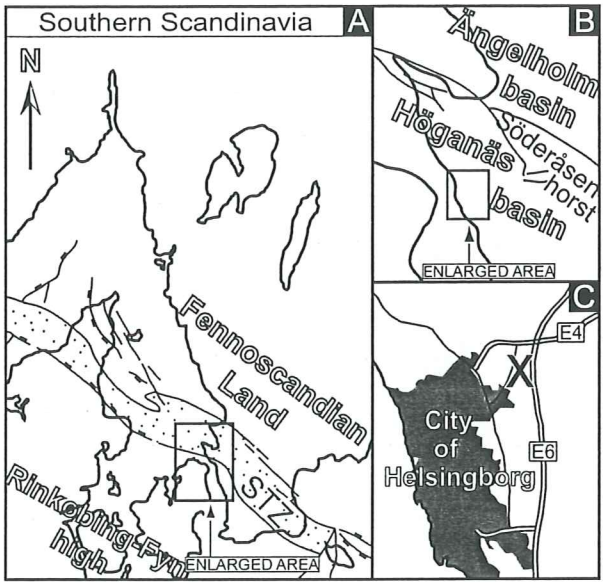

Fig.1. A. Southern Scandinavia with the Sorgenfrei-Tornquist Zone (STZ) along the Fennoscandian Border Zone. B. The Höganäs basin. C. Helsingborg city and the Filborna well site (marked X).

A comprehensive review of the Upper Triassic and Jurassic geology in Skåne, southern Sweden, was presented by Norling *et al.* (1993). They described the Jurassic deposits and the fault-bounded basins, as being strongly influenced by Late Cretaceous tectonic activities within the Sorgenfrei-Tornquist Zone. Thermal Alteration Index and vitrinite reflectance data indicate that the basins probably never reached temperatures higher than 70 – 90°C (Norling *et al.* 1993, p.16). Consequently the basins never reached a depth of more than 2000 metres (Norling & Bergström 1987; Norling *et al.* 1993). These basins were the catchment areas for sediments from the nearby horsts and the sedimentary successions from the Late Triassic to Middle Jurassic reflect a radical climatic change (Norling *et al.* 1993). The Norian Kågeröd Formation consists of clastic red-beds that are minimally weathered and texturally immature, it was deposited in a continental environment under semi-arid conditions. At the onset of the Rhaetian, the climate shifted, leading to more humid environments, giving rise to a dramatically increased chemical weathering as CO_2-rich acidic water flushed the soils, supporting the formation of kaolinite and completely suppressing the formation of smectite (Ahlberg 1994). The accumulation of autochthonous coal and kaolinitic argillites in the deltaic successions was promoted by weathering in the Rhaetian-Hettangian, i.e. the Höganäs Formation. According to Norling *et al.* (1993) the Rhaetian-Het-

	Stages	Lithostratigraphy	
Jurassic	Sinemurian	Rya Fm	Döshult Mb
Jurassic	Hettangian	Höganäs Fm	Helsingborg Mb
Triassic	Rhaetian	Höganäs Fm	Bjuv Mb
Triassic	Rhaetian	Höganäs Fm	Vallåkra Mb
Triassic	Norian	Kågeröd Fm	Not subdivided

Fig.2. The lithostratigraphic units at the Triassic-Jurassic boundary in NW Skåne.

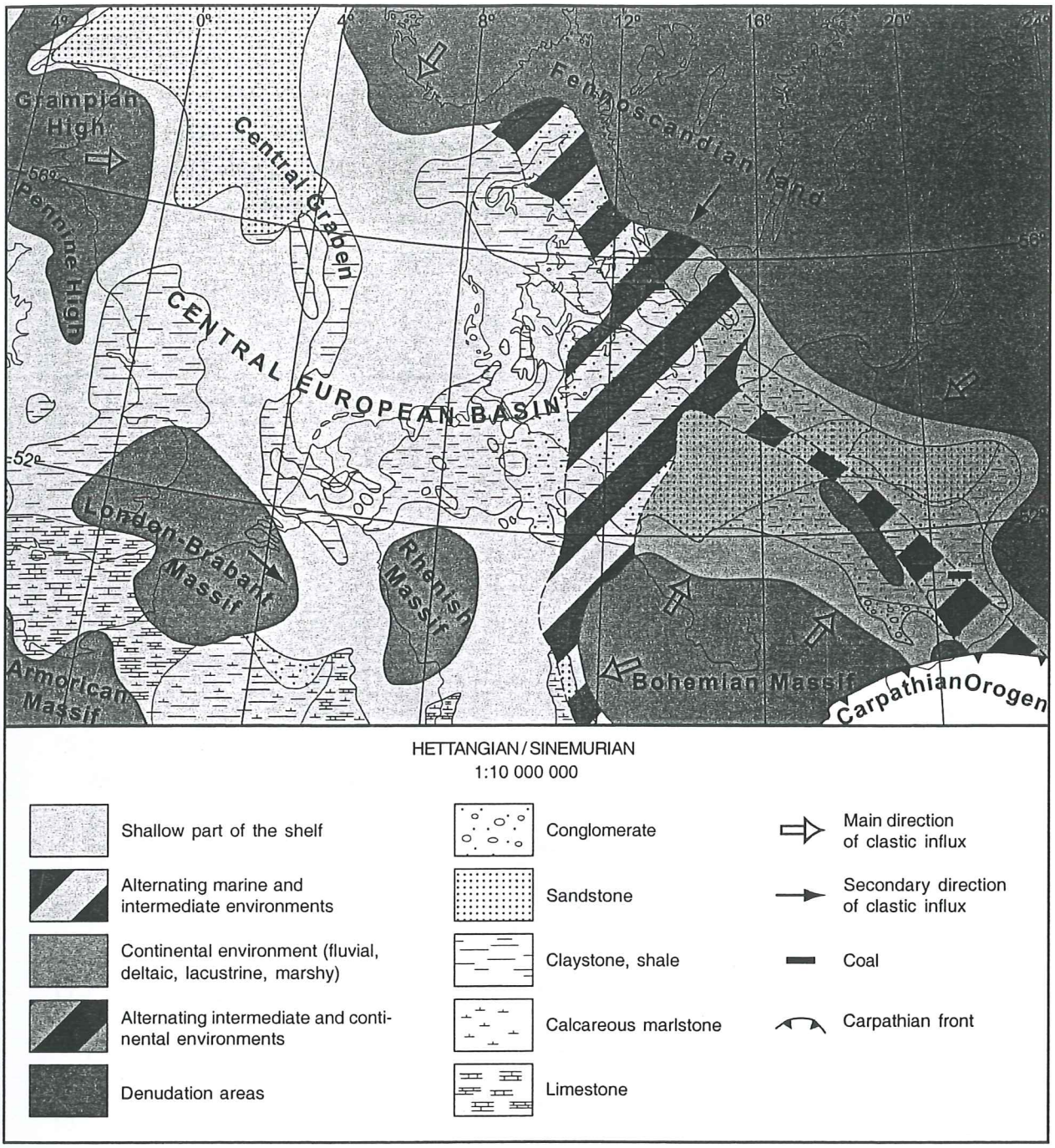

Fig.3. Lower Jurassic (Hett.-Sin.) lithologic-palaeogeographic map over Europe. After Grigelis and Norling (1999).

tangian sediments were deposited in alluvial-deltaic settings (Fig 3), which together with the increased chemical weathering caused the textural maturity to become relatively high. Troedsson (1950, 1951) divided the Helsingborg Member into twelve depositional cycles, where the origin of these cycles is not fully understood, but Troedsson (1950, 1951) suggested a theory where the cyclisity was the product of repeated subsidence pulses due to tectonic activity. A more recent explanation relates the cycles to eustatic sea-level changes (see Ahlberg *et al.* 2001).

The main objective in this study was to examine the petrophysical anisotropy in plugs obtained from the NSR drill cores in order to analyse the permeability differences in horizontal and vertical directions (i.e. along and perpendicular to bedding), and to correlate the anisotropy to petrographic and sedimentological features of the strata. Questions related to reservoir heterogeneity important to the petroleum exploration industry are addressed because the heterogeneity in reservoir sand bodies causes anisotropy during petroleum production. Macro-scale anisotropy is notified when large sand bodies are encased by impermeable strata or fault zones. Heterolithic sand/mud stratification is the predominant contributor to anisotropy in meso-scale, whereas grain shape and grain orientation control micro-scale anisotropy. Hence, the anisotropy of a reservoir is controlled by the depositional and diagenetic settings and will control the hydrocarbon migration within it.

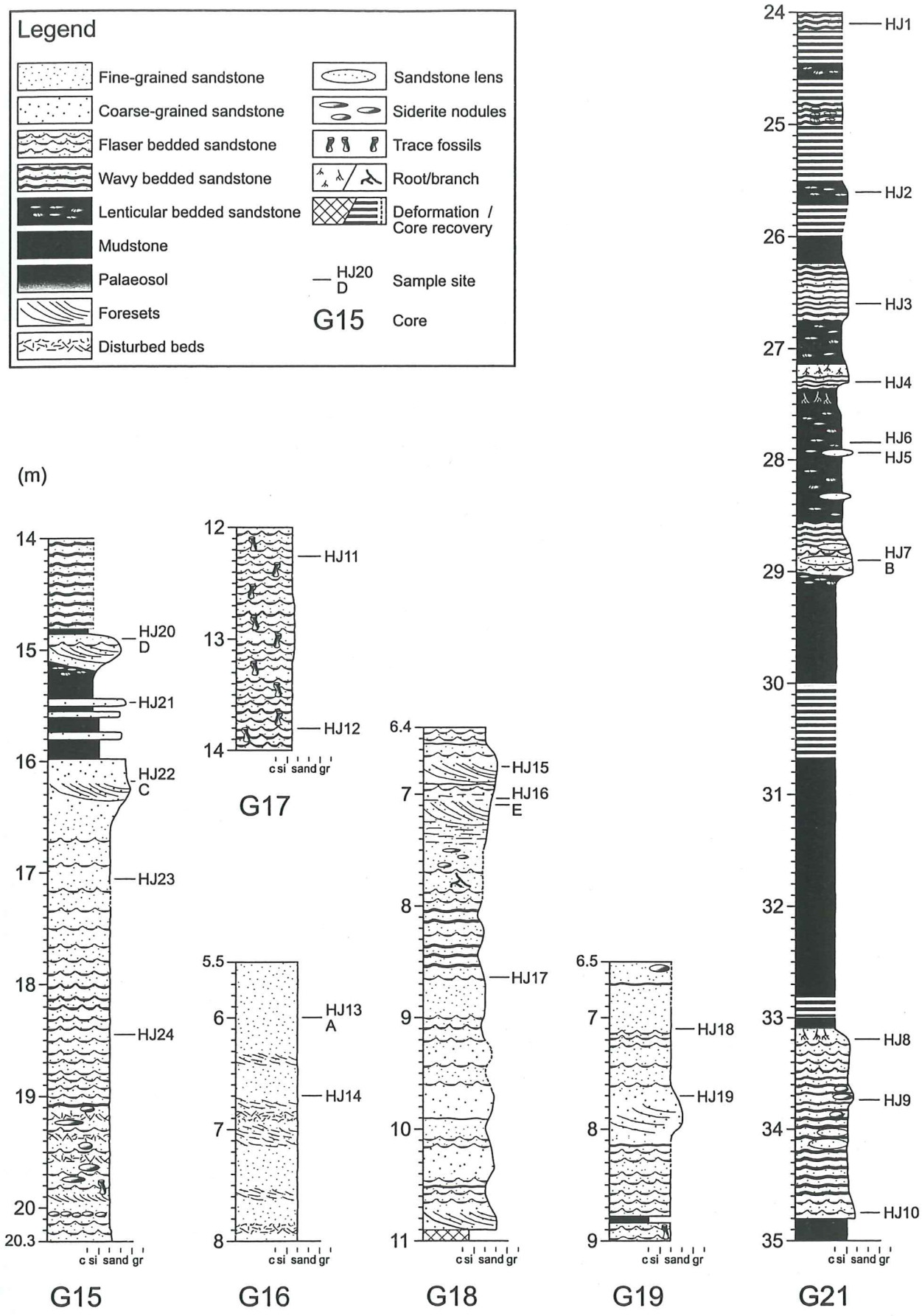

Fig. 4. Logs of the studied cores. Lengths are in meters.

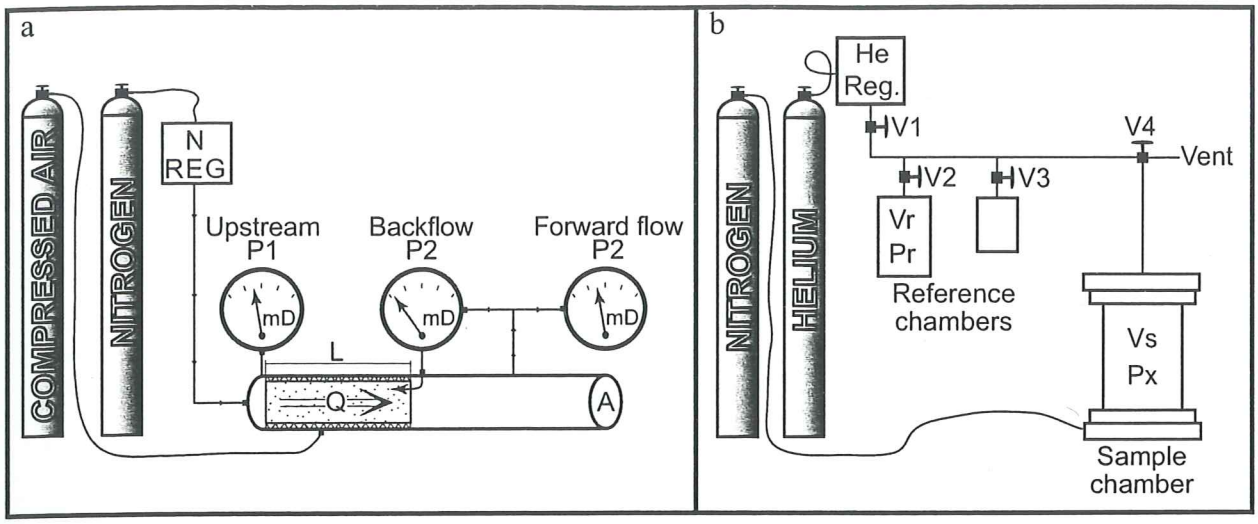

Fig.5. Sketch describing the techniques of the permeameter and the porosimeter. N=Nitrogen, L=Length, Q=Flow, A=Area, REG=Regulator, He=Helium, V =Volume, Vr=Reference volume, Pr=Reference pressure, Vs=Volume of sample chamber, Px=Expanded pressure.

Material

The samples (HJ1-HJ24) were collected from 24 places in six of the NSR cores for analysis of permeability, porosity and sedimentary petrography (Fig 4). The studied sedimentary successions (cores) have a total length of 28.9 m and each core is between 2 and 11 m in length. The cores are designated G15 – G19 and G21. Plugs for permeability and porosity measurements were taken from all cores, both in vertical and horizontal directions. All thin sections (HJ1-HJ24) were examined in polarised-light microscope and subjected to backscatter image analysis (including BSE image point-counting) and cathodoluminescence microscopy (CL). Additional samples were prepared for secondary electron imaging (SEI). Five clay fraction samples from homogeneous sandstone beds, which did not contain any macroscopically visible amounts of detrital clay, were selected for X-ray diffraction (XRD) analyses.

Table 1. Number of samples analysed in the study.

Method	Number of samples
Permeability and Porosity	38
Polarised-light microscope	24
Backscatter image analysis	21
Point counting	42
Cathodo luminescence	21
X-ray diffraction	5
Secondary electron imaging	24

Methods

Permeability and porosity

Where the limited lithification permitted, permeability and porosity plugs were drilled from each core and from all different facies. Samples taken from wavy- and lenticular-bedded heteroliths were particularly difficult to obtain, due to their sand/mud interlamination (heterogeneous consolidation). Thirty-eight plugs were used for permeability and porosity measurements, being drilled parallel and perpendicular to bedding to investigate permeability anisotropy. The plugs were dried in an oven at 105°C for 48 hours, weighed, and their lengths and diameters were measured for plug volume calculations (V_B), to facilitate the operation of the porosity and permeability instruments (Fig 5). To obtain accurate results the plugs must have a diameter of 1 inch and a minimum length of 1 inch. Preferably the plugs should be longer than 2.5 centimetres, up to 7 centimetres long. In order to fill the sample chamber, when measurements were carried out on plugs shorter than 4.5 centimetres, stainless steel filler-plugs (1", 1½", 2" long) were added. Before operating the instrument, a reference chamber is selected, depending on which filler-plug is used. The effective porosity was measured in a Helium Gas Expansion Porosimeter (Fig 5b), made by Edinburgh Petroleum Services (EPS). To obtain porosity results, the plugs were subjected to compressed nitrogen gas in a sample chamber with the known volume V_S. One of the two reference chambers was filled with helium gas to produce a reference pressure (P_R) and the value was registered. The helium gas introduced into the sample chamber and a new value was obtained (P_X). A modified version of Boyle´s law was used for the porosity calculation:

$P_R \cdot V_R = P_X(V_R + V_S - V_G)$

Where:

P_R = reference pressure (psig)

V_R = reference volume (cm^3)

P_X = expanded pressure (psig)

V_G = grain volume (cm^3)

V_S = volume of sample chamber (cm^3)

The volume of sample chamber (V_S) is dependant on the choice of filler plug. Rearranging Boyle´s law gives the following equation:

$$V_G = V_R + V_S - (V_S - P_R)/P_X$$

The effective porosity is obtained from:

$$\Phi = (V_B - V_G)/V_B$$

Where V_B is the bulk volume measured in cm^3.
The absolute permeability was then measured in an EPS Digital Gas Permeameter (Fig 5). To determine the permeability Darcy´s law was used:

$$Q = K \cdot A \cdot (\Delta P / L)$$

Where Q is the flow rate; A is the area of the cross section that the gas passes through; ΔP is the pressure difference (P_1-P_2) measured over the length (L) of the sample. K is the hydraulic conductivity that is dependent on the permeability (k) as:

$$K = k \cdot \rho \cdot g / \mu$$

Where: ρ is the density, μ is the nitrogen viscosity of the gas/liquid and g is the gravity. Nitrogen is sent through the sample and the average gas flow rate Q_M, average pressure P_M ($\frac{1}{2}P_1 + \frac{1}{2}P_2$) and pressure difference ΔP over the sample is measured. From this the gas-permeability is found by the equation:

$$Kg = L \cdot Q_M \cdot P_A / \rho \cdot g \cdot A \cdot P_M \cdot \Delta P$$

Where P_A is the atmospheric pressure, P_A (atm) = P/760 (mmHg)

FORWARD FLOW:

$P_1 = \Delta P / 14.7 + P_A$

$P_2 = P_A$

BACK FLOW:

$P_1 = Pi/14.7 + P_A$

$P_2 = (Pi - \Delta P)/14.7 + P_A$

Measurements were done at three levels of upstream pressure in cases of forward flow, and at backward flow five different upstream pressure levels were used. Using a linear least square method the ordinate on the y-axes was calculated to obtain the absolute permeability. If measurements did not conform to a straight line (R>0.95), then they were repeated or changed to back flow measurement. With the equipment used in this study, measured permeability values below 1 mD are considered to be unreliable.

Backscatter electron microscopy and point-counting

To improve the accuracy of conventional polarised-light microscopy point-counting, all thin-sections were examined by means of backscattered electron microscopy (BSE). In this method the density is mapped and reproduced as a grey scale (white = heavy, black = light). Trewin (1988) gives a more detailed description of the technique of the backscatter electron microscope. The approach of the BSE point-counting was to achieve a more accurate result and particularly for grain sizes smaller than medium-grained sand, which are difficult to distinguish in a light microscope (Cooper *et al.* 2000). Two representative fields of view from each thin-section were photographed, printed at uniform size and nine categories of components were point-counted using a transparent grid (two fields of view x 391 points). The point-counting data were further used to classify the arenites in a QFL-diagram (see Dott 1964). Examinations of feldspar dissolution, texture and heavy minerals were also carried out.

Cathodoluminescence microscopy

Thin sections were surveyed by the means of cathodoluminescence (CL) after BSE examination, in a cathodoluminescence vacuum chamber placed on a conventional transmitted polarised light microscope. Cathodoluminescence is produced when electrons bombard the thin-section surface and is expressed as emission of visible light. The CL reproduces a visible intensity spectrum (colour), which reflects differences in crystal lattice perfection (Miller, 1988). Quartz overgrowths have almost perfect crystal lattices, since they were formed under lower pressure and temperature than the detrital quartz grains were, hence, quartz overgrowths have a non-luminescent appearance (Owen, 1991). In order to distinguish quartz grains from quartz overgrowths, all thin-sections were photographed both by means of CL and conventional microscope to obtain micrographs from the equivalent field of view.

Secondary electron imaging

Secondary electron imaging (SEI) of fractured samples was used to obtain good, three-dimensional overviews of the content and distribution of the mineral phases and pores in the sample (cf. Trewin 1988). To achieve this, freshly broken rock pieces were glued on stubs and sputtered with gold. Carbon was added on the sides of the sample to ensure electrical conductivity between the gold and the stub.

X-ray diffraction

To analyse the diagenetic clay mineralogy of the porous sandstones, samples were obtained at five selected locations from different cores (Fig 4). Four of them were collected at core depths coinciding with the HJ sample series

Sample	Core	Level	F.C.	Density	Poro.(%)	Perm. (mD)	ALMA Index
HJ1h	G21	24,10	W	2,66	14,2	low	
HJ1v				2,66	14,9	3.95*	
HJ2h	G21	25,60	L	no sample			
HJ2v				no sample			
HJ3h	G21	26,60	W	2,67	17,6	22,28	0,007
HJ3v				2,68	17,8	0,16	
HJ4h	G21	27,30	W(L)	no sample			
HJ4v				2,68	12,2	0.05*	
HJ5h	G21	27,95	L	2,66	1,5	low	
HJ5v				2,67	2,1	low	
HJ6h	G21	27,85	L	2,85	14,1	low	
HJ6v				2,88	12,5	low	
HJ7h	G21	28,90	F	2,64	14,4	21,35	0,395
HJ7v				2,65	13,8	8,43	
HJ8h	G21	33,20	F	no sample			
HJ8v				2,60	9,6	0.11*	
HJ9h	G21	33,75	L	3,00	13,5	0,04	30,339
HJ9v				2,95	13,4	1.28*	
HJ10h	G21	34,75	F	not measured		44,97	0,591
HJ10v				2,64	16,5	26,59	
HJ11h	G17	12,25	F	2,66	17,9	22,86	0,011
HJ11v				2,66	19,3	0,26	
HJ12h	G17	13,80	F	2,68	19,2	62,30	0,003
HJ12v				2,66	18,6	0,16	
HJ13h	G16	6,05	Sh	2,65	31,6	3654,43	0,982
HJ13v				2,66	31,8	3588,89	
HJ14h	G16	6,70	Sh	2,64	30,2	2537,76	0,844
HJ14v				2,65	31,2	2141,13	
HJ15h	G18	6,75	Sh	2,64	30,5	4904,05	0,412
HJ15v				2,65	26,5	2020,25	
HJ16h	G18	7,05	Sh	no sample			
HJ16v				2,64	31,4	6035,37	
HJ17h	G18	8,65	F	no sample			
HJ17v				2,67	23,1	9,45	
HJ18h	G19	7,10	Sh	2,63	30,9	5375,06	0,540
HJ18v				2,64	28,0	2903,28	
HJ19h	G19	7,70	F	2,70	12,1	0,33	0,112
HJ19v				2,73	11,2	0,04	
HJ20h	G15	14,90	F	2,64	30,1	3425,78	0,580
HJ20v				2,65	27,0	1987,98	
HJ21h	G15	15,45	W	no sample			
HJ21v				2,65	23,8	1854,04	
HJ22h	G15	16,15	Sp	no sample			
HJ22v				no sample			
HJ23h	G15	17,05	F	2,87	28,2	675,33	0,217
HJ23v				2,64	26,8	146,77	
HJ24h	G15	18,45	F	2,62	22,3	155,00	0,001
HJ24v				2,60	21,7	0,13	

Table 2. Permeability and porosity measurements and sample location from respectively core. Density values and ALMA-index are also listed. Asterisks mark that only the first measured point is used and permeability are lower than values.

and all samples were named A – E respectively. The sandstones were gently disintegrated and the clay fractions isolated by means of settling. The clay fraction (< 2 micron) was then used to produce oriented XRD slides. The untreated slides were first analysed by means of XRD and then again after being heated to 550°C for two hours. The heating was carried out in order to discriminate overlapping XRD peaks between minerals, which would otherwise be misinterpreted. At the temperature of 550° C, the crystal structure of kaolinite breaks down completely, whereas coinciding chlorite peaks remain unaffected. In two instances samples were analysed, after pretreatment with ethylene glycol (EG). The EG-method expands smectite lattices, and facilitates XRD peak identification.

Result

Descriptions of cores

The core G15 is dominated by flaser-bedded, fine-grained sandstone (Fig 4). The lower part of the core shows features such as siderite nodules and disturbed stratification (water escape structures). The occurrence of the disturbed stratification takes place in a cyclic order, with 20 centimetres inter-distance. Mud drapes occur within the flaser-bedded sandstone and were also deposited in a cyclic order with an inter-distance of 10 centimetres. The core consists of two bedsets of trough-crossbedded coarse-grained sandstone. One siderite cemented bed is observed in the lower part of the core together with a trace fossil. Samples taken from this core include: HJ24 at 18.45 m, HJ23 at 17.05 m, C and HJ22 at 16.15 m, HJ21 at 15.45 m, and D and HJ20 at 14.90 m.

The core G16 is dominated by homogeneous, fine-grained sandstone, which lacks visible stratification. At 7.9 m and between 7.6 to 6.5 m thin mud laminae drapes the foresets. At 7.9 m and 6.9 to 6.8 m disturbed layers (dewatering structures) are visible due to the presence of mud drapes. Samples taken from this core include: HJ14 at 6.7 m, and A and HJ13 at 6.05 m.

The core G17 consists of flaser-bedded, fine-grained sandstone to siltstone. Trace fossils were observed throughout the core. Compared with the flaser bedded sandstones from G15, the mud drapes in G17 are more condensed and thicker, and the cyclic order is therefore not as apparent. Samples taken from this core include: HJ12 at 13.8 m and HJ11 at 12.25 m.

The core G18 is dominated by flaser-bedded, medium- to fine-grained sandstone. Three trough-crossbedded bedsets have been observed. In the middle part of the core, the content of mud laminae is notable. Wavy-bedded sandstone beds with root traces have been observed, as well as thin coal seams. Siderite nodules were observed at the level between 8 and 7 metres. Samples taken from this core include: HJ17 at 8.65 m, E at 7.10 m, HJ16 at 7.05 m, HJ15 at 6.75 m.

The core G19 is dominated by flaser-bedded, fine-grained sandstone, with prominent mud-drapes in the lower part. At the central part of the core is a medium- to coarse-grained sandstone trough-crossbedded bedset. Siderite nodules and calcite cemented beds are common in the upper part of the core. Small trace fossils were observed near the base of the core. Samples taken from this core include: HJ19 at 7.7 m and HJ18 at 7.1 m.

The core G21 is dominated by mudstone. However, at the base and in the middle of the core, flaser-bedded sandstone and sand lenses occur. A mature palaeosol and several root horizons were identified, as well as several poorly developed palaeosols. Siderite nodules are common in the flaser-bedded sandstone and the mud drapes are typically completely cemented by siderite. Fine-grained sandstone lenses are observed in the flaser-bedded sandstone and within the mudstone. Samples taken from this core include: HJ10 at 34.75 m, HJ9 at 33.75 m, HJ8 at 33.2 m, B and HJ7 at 28.9 m, HJ5 at 27.95 m, HJ6 at 27.85 m, HJ4 at 27.3 m, HJ3 at 26.6 m, HJ2 at 25.6 m, HJ1 at 24.1 m.

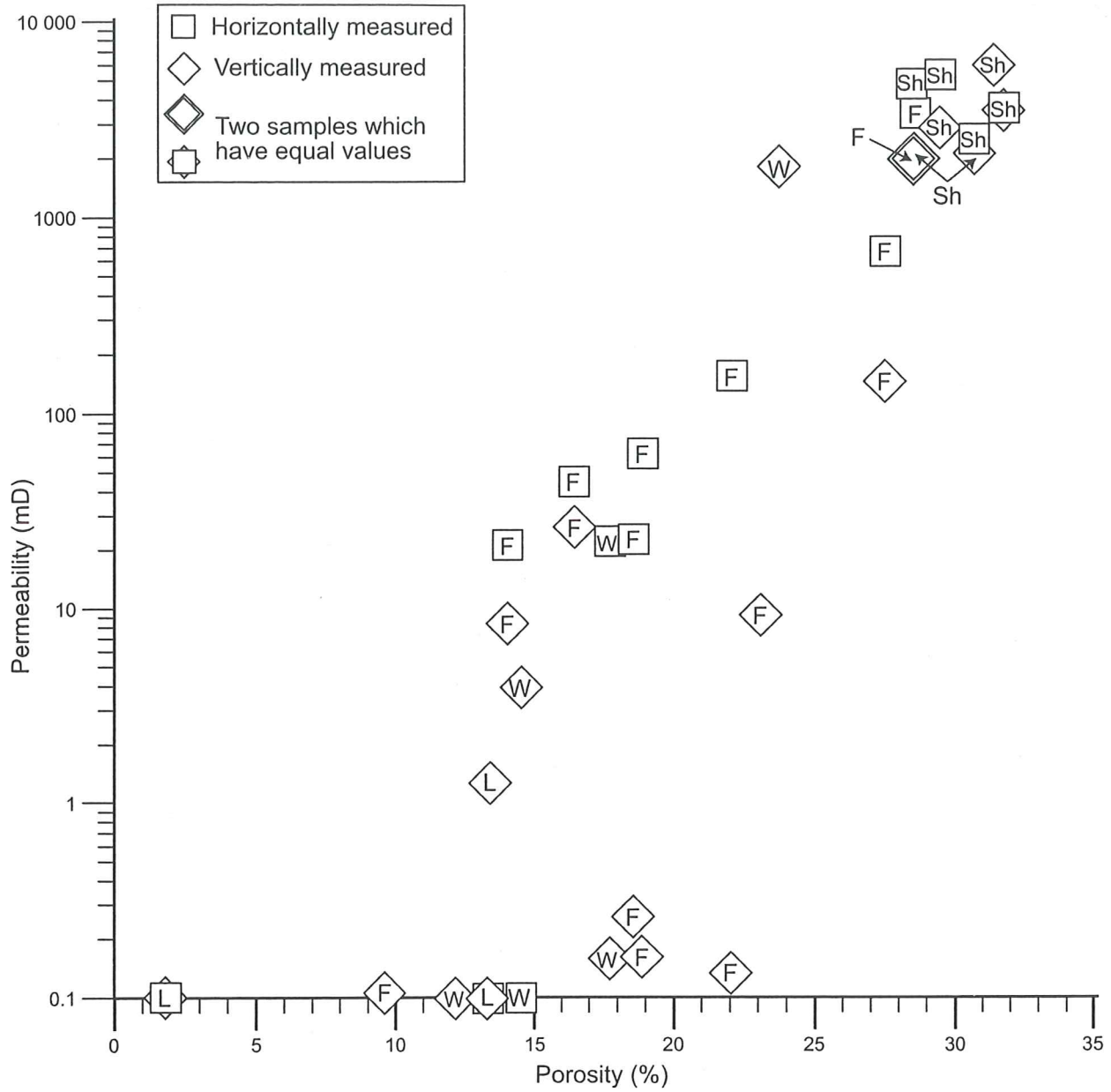

Fig. 6. Cross plot of porosity vs. permeability of 38 samples with their facies code. Sh=Homogeneous sandstone, F=Flaser bedded sandstone, W=Wavy bedded sandstone, L=Lenticular bedded sandstone.

Permeability and porosity

Measurements on permeability and porosity were completed on all 38 plugs (Table 2). The measurements are cross-plotted against porosity together with the facies code (Fig 6). The cross-plot illustrates that homogeneous sandstone are the most permeable group both in horizontal and vertical directions. Flaser-bedded sandstone is the most significant group with differences in horizontal and vertical direction, thus the group has a wide permeability range. All samples, measured horizontally as well as vertically, showed a preferred permeability in a horizontal direction, except from one (Fig 7). The vertical-lateral difference in permeability is not equivalent with the permeability anisotropy, since this does not reflect the magnitude of the anisotropy. To visualise this problem an index was created, Analysis of Linear Measured Anisotropy (ALMA), where the anisotropy is the quotient of vertically versus horizontally measured permeability (Table 2; Fig 8). If compared the samples HJ10 and HJ18 have a pronounced difference in permeability, HJ10 has approximately 18 mD in difference and HJ18 has approximately 2470 mD in difference. When compared using the ALMA index, sample HJ10 is more isotropic (0.59) than sample HJ18 (0.54). The most pronounced anisotropy was found in those samples that contain mud laminae, however, samples from homogeneous sandstones also clearly show heterogeneity. Sample HJ9 has a lower measured permeability in a horizontal than in a vertical direction due to abundant siderite cement in both plugs. However, for permeability values below 1 mD, such as sample HJ9, the data is unreliable. Fourteen of the samples show permeability below 1 mD and in 5 of the samples (Table 3, "low") the accurate data was unobtainable. Because of the negligi-

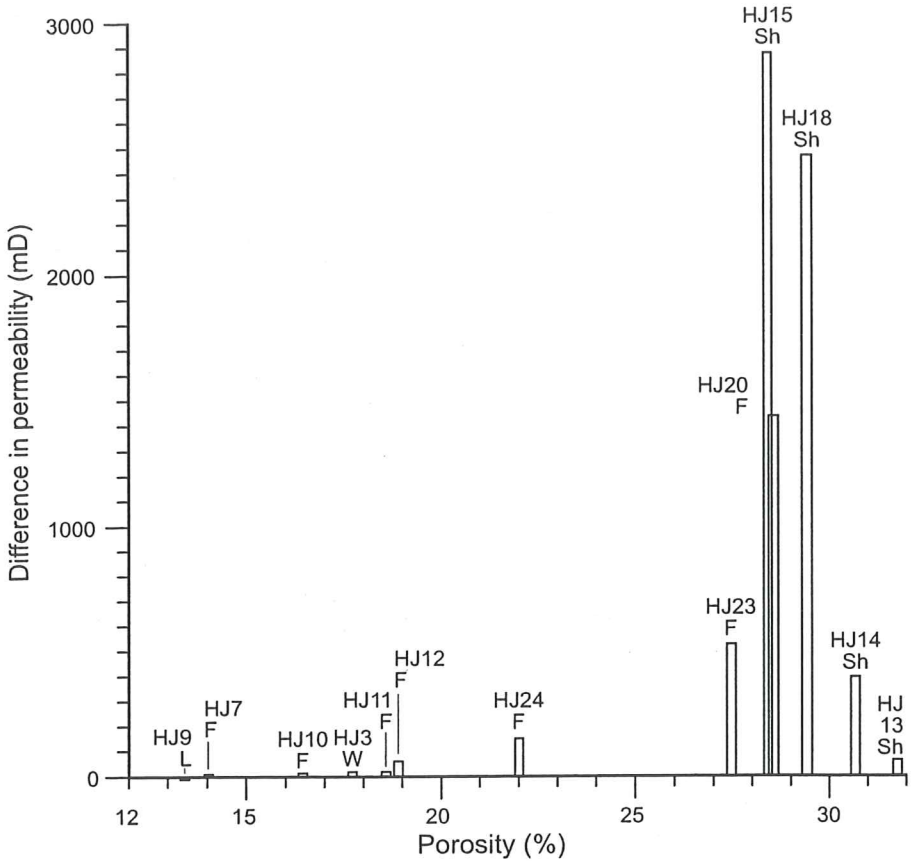

Fig.7. Bar chart to visualise the permeability difference in 26 samples with a porosity range between 12 to 32 per cent. L=Lenticular bedded sandstone, W=Wavy bedded sandstone, F=Flaser bedded sandstone, Sh=Homogeneous sandstone.

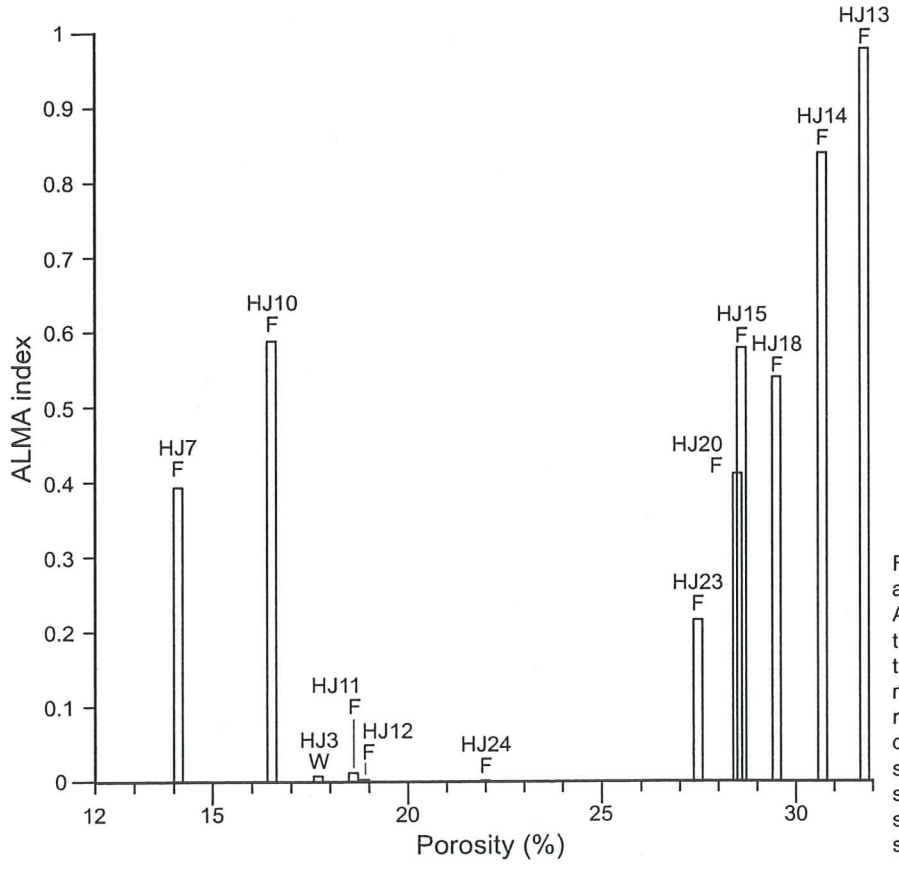

Fig. 8. Bar chart to visualise the anisotropy in 24 samples with an ALMA-index.The ALMA-index is the quotient of vertical permeability divided with the horizontal permeability. The samples have a porosity range between 12 to 32 percent. L=Lenticular bedded sandstone, W=Wavy bedded sandstone, F=Flaser bedded sandstone, Sh=Homogeneous sandstone.

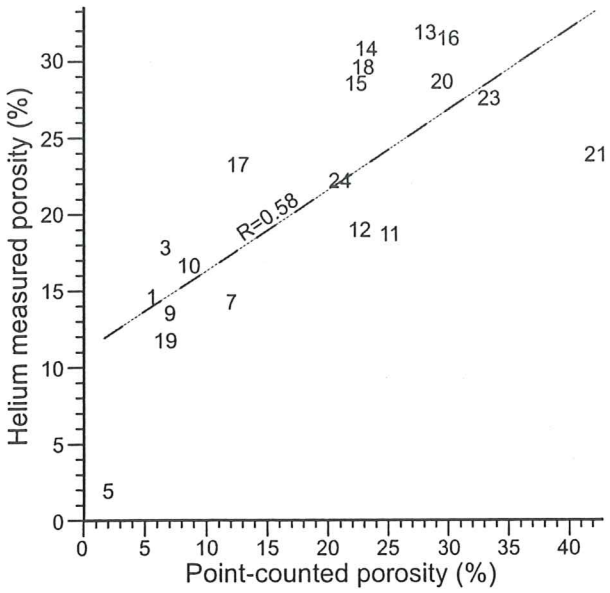

Fig. 9. Cross plot of point-counted porosity vs. helium measured porosity. Dotted line represents the correlation between the samples.

ble values all 14 can be classified as having negligible permeability. Sample HJ10h has not been measured by means of porosity and density since it was assumed that this sample has the same values as HJ10v.

Correlation between point-counted porosity and porosity measured with porosimeter (Fig 9) demonstrates that porosity interpretation with point-counting by means of BSE is a reliable method. In samples with low porosity, the EPS porosimeter measures micro porosity, whereas point-counted micro porosity is immeasurable due to resolution problems.

Petrography

Point-counting

Twenty-one thin-sections were examined and point-counted by means of BSE (Table 3). The grains in all thin-sections have sub-angular to sub-rounded shapes, and 15 of them are classified as subarkoses whereas six samples are classed as quartz arenites (Fig 10). The thin-sections vary in their content of clay- and feldspar, carbonate cement (Table 3) and grain size (Fig 11). The point-counted mud matrix from all thin-sections is considered to be of detrital origin. The mud matrix content correlate well with the majority of samples with negligible permeability (HJ1-HJ3, HJ7, HJ9-HJ12, HJ17 and HJ24), i.e., where the mud content is more than 3 percent. The samples HJ5 and HJ19 are calcite cemented which has caused a severe porosity and permeability reduction. The permeability of the samples HJ14 and HJ15 is almost unaffected by the mud matrix, probably because of the low matrix content, but show a noticeable permeability difference in horizontal and vertical directions.

Sample	Quartz	Feldspar	Rock fragment	Mud matrix	Calcite	Mica	Other	Fe-oxide	Point-counted Porosity	Helium measured Porosity	Horizontal Permeability	Vertical Permeability	Classed
HJ1	72,3	4,9	0,3	16,8		0,3		0,3	5,4	14,5	Low	3.95*	S.A.
HJ2	58,6	5,5		32,0		0,3		0,9	2,8				S.A.
HJ3	76,6	8,5	0,5	7,0				0,9	6,5	17,7	22,28	0,16	S.A.
HJ4	No thin section									12,2		0.05*	
HJ5	62,6	6,3		1,7	26,5			1,0	1,9	1,8	Low	Low	S.A.
HJ6	No thin section									13,3	Low	Low	
HJ7	80,1	2,6	0,6	3,7				1,2	11,9	14,1	21,35	8,43	Q.A.
HJ8	No thin section									9,6		0.11*	
HJ9	67,3	5,2		17,9		1,0		1,7	6,9	13,4	0,04	1.28*	S.A.
HJ10	65,1	4,2		20,1		1,4		0,9	8,3	16,5	44,97	26,59	S.A.
HJ11	62,7	4,0	2,3	5,5				0,6	24,9	18,6	22,86	0,26	S.A.
HJ12	64,8	5,1	0,8	6,3				0,8	22,3	18,9	62,30	0,16	S.A.
HJ13	67,8	2,1	0,5				1,9		27,8	31,8	3654,43	3588,89	Q.A.
HJ14	67,5	3,2	1,3	1,7			2,7	0,8	22,9	30,7	2537,76	2141,13	S.A.
HJ15	73,2	2,1	0,6	0,4			1,3	0,5	22,0	28,5	4904,05	2020,25	Q.A.
HJ16	65,1	1,2					3,8	0,1	29,8	31,4		6035,37	Q.A.
HJ17	61,5	4,7	0,6	12,3		0,4		8,2	12,3	23,1		9,45	S.A.
HJ18	71,4	1,9	0,4				3,1	0,6	22,6	29,5	5375,06	2903,28	Q.A.
HJ19	58,8	5,6	0,3	2,6	25,6		0,8		6,4	11,6	0,33	0,04	S.A.
HJ20	64,1	4,2	0,3				2,1	0,3	29,2	28,6	3425,78	1987,98	S.A.
HJ21	50,9	5,1						1,8	42,2	23,8		1854,04	S.A.
HJ22	51,3	5,4					2,4	0,6	40,3				S.A.
HJ23	60,7	2,6					2,7	0,9	33,1	27,5	675,33	146,77	Q.A.
HJ24	59,6	6,1	0,1	6,0	0,0	0,9	5,9	0,6	20,7	22,0	155,00	0,13	S.A.

Table 3. Results of BSE-point-counting on slides and permeability and porosity measurements. Asterisks mark that only the first measured point is used and permeability are lower than values.

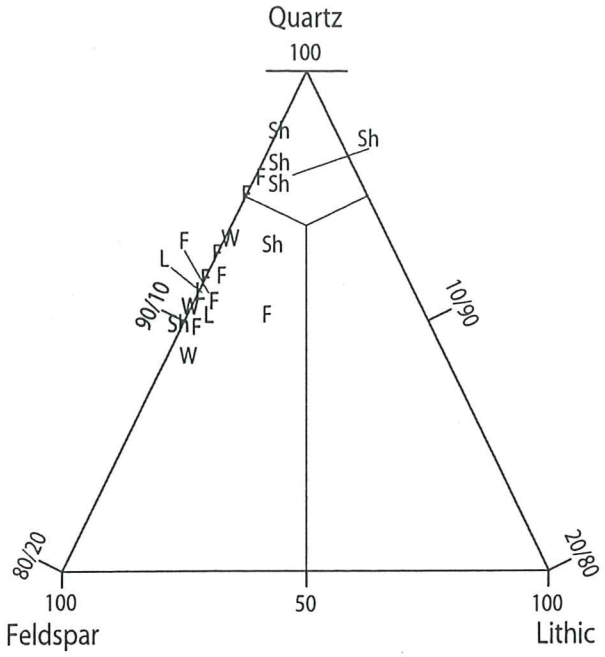

Fig. 10. Point-counted samples (n=21) and facies codes are plotted in QFL-diagram. L=Lenticular bedded sandstone (3), W=Wavy bedded sandstone (3), F=Flaser bedded sandstone (9), Sh=Homogeneous sandstone (6).

Quartz overgrowths

Cathodoluminescence (CL) and secondary electron imaging (SEI) were used to identify quartz overgrowths. When examined in SEM almost all the samples showed thin quartz overgrowths with euhedral faces. Six of the samples with low permeability (HJ3, HJ7, HJ11, HJ12, HJ17 and HJ24) have the thickest quartz overgrowths. These samples have noticeable amounts of partly dissolved feldspar, a feature rarely seen in the more permeable samples with low amounts of quartz overgrowths. In some samples, authigenic kaolinite and authigenic micro quartz were observed adjacent to the dissolved feldspars (Fig 12a,c). This implies that quartz precipitated rapidly from over saturated pore fluids at times (Jahren & Ramm 2000). However, most quartz overgrowths are euhedral extensions of quartz grains and were formed more slowly during gradual pore water evolution (Fig 12). The limited quartz cement content proved to be difficult to detect by means of CL (Fig 11e). Only sample HJ15 showed quartz overgrowths when examined with CL (Fig 11f), however, when examined in SEI (stub), sample HJ15 was among the samples with the least quartz overgrowths. There are a number of trace elements that may extinguish the luminescence or reduce the luminescence intensity (Budd *et al.* 2000). Relief in samples also causes problems with detecting quartz overgrowth. If thin-sections are sufficiently polished, the CL electron gun that shoots electrons at an angle onto the sample will reproduce a structure, which could be misinterpreted as overgrowths (Fig 11g).

Carbonate cementation

Carbonate cementation occur in several samples of the studied material, mostly as siderite nodules and siderite cemented layers (Fig 4). Two of the thin-sections, HJ5 and HJ19, showed large amounts of poikilotopic calcite cement when examined under the polarised-light microscope and they were the only samples from the investigated cores that contain calcite cement (Fig 11d), however, in sample HJ14 there is small amounts of authigenic carbonate (Fig 12h). Sample HJ19 has a higher porosity than sample HJ5, which can be related to a difference in grain size due to different depositional environments; HJ5 is sampled in a fine-grained sandstone lens, and HJ19 is sampled in medium-grained, trough-crossbedded sandstone.

Clay mineralogy

All five clay-fraction samples show similar XRD patterns (Fig 13). All samples show strong kaolinite 001 and 002 reflections when analysed untreated. These peaks disappeared in all the samples after heating to 550°C (no chlorite was detected). The untreated samples also show a group of smaller peaks, which were stable after heating, around 10.0 Å, 5.0 Å, and 3.0 Å, i.e., the 001, 002 and 003 reflections of illite. Two slides (sample C and D) were subjected to EG-pretreatment without any detection of expandable clay minerals.

Discussion

The permeability data clearly show that anisotropy occurs in all six drill cores and in all facies. The cause of anisotropy can be referred both to the direct effects of deposition as well as to the diagenesis. The heteroliths and the mudstones are formed during periods of slack water condition that is typical for tide-dominated deltaic environments. Variation in physical turbulence both in the lacustrine and in the marine water, caused mud particles to settle and form impermeable mud drapes in otherwise turbulent sandy environment. In Fig 6 increasing mud drape density of different heterolithic types illustrates a negative impact on porosity and permeability. At places this impact is so apparent that it potentially constitute the main control on the reservoir quality.

However, of the observed diagenetic features, carbonate and quartz cementation caused the greatest permeability and porosity reduction after deposition, and locally strata-bounded carbonate cement replaced the intergranular porosity totally. Carbonate cementation can be rapid and lithification of sediments may take place in a matter of decades (Friedman 1998). Siderite cement precipitates early in the eogenesis, preferably in fine-grained floodplains, crevasse splays, oxbow lakes and in pond sediments (Morad 1998). Within the studied material, siderite cement occurs mostly in the mud drapes and has enhanced the permeability anisotropy. However, the siderite cement in the cores is a limited reducing factor of the total permeability and porosity, although it can locally serve as a pore filling cement. Two of the samples, HJ5 and HJ19, are almost completely cemented by poikilotopic calcite and conse-

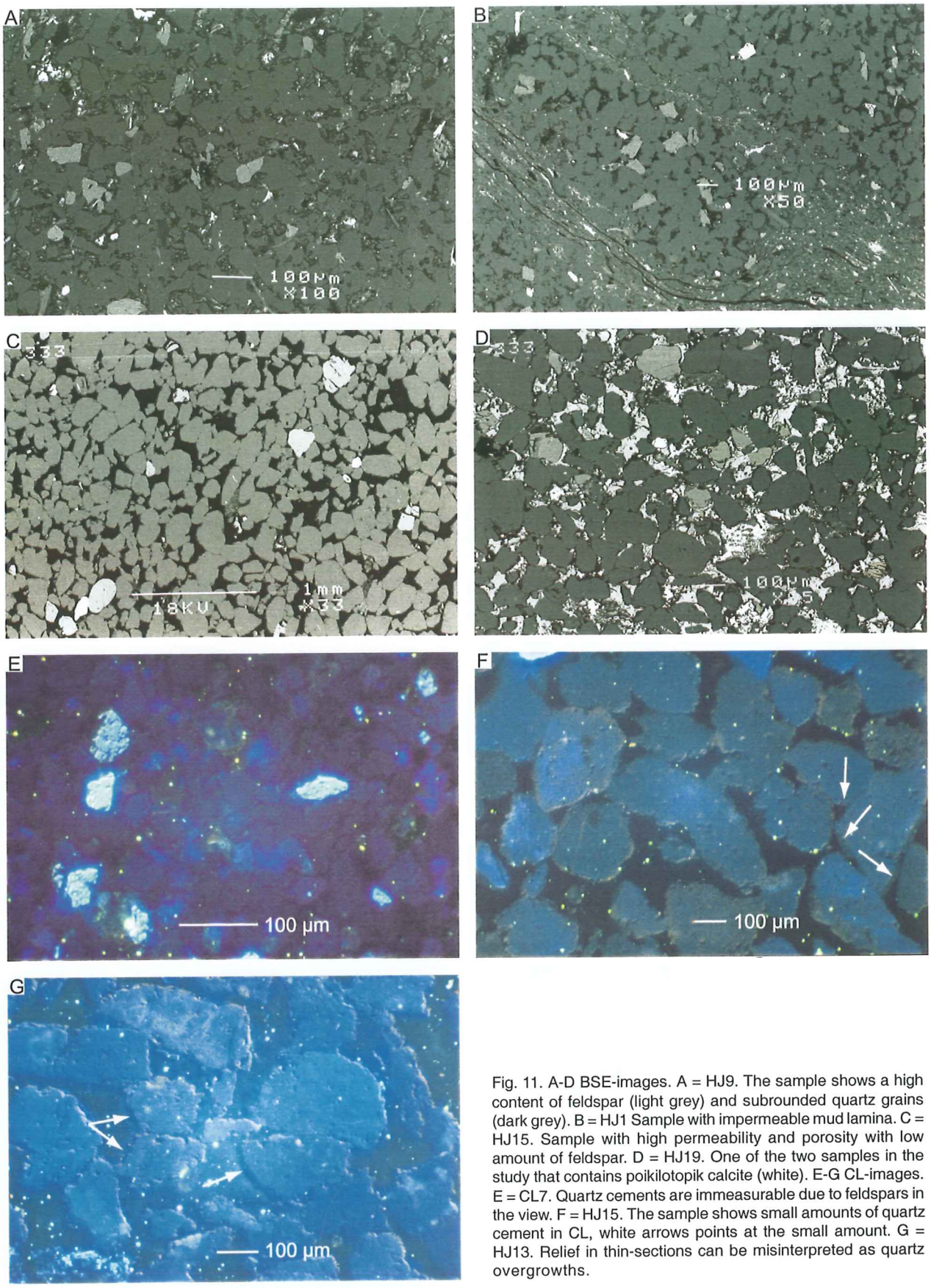

Fig. 11. A-D BSE-images. A = HJ9. The sample shows a high content of feldspar (light grey) and subrounded quartz grains (dark grey). B = HJ1 Sample with impermeable mud lamina. C = HJ15. Sample with high permeability and porosity with low amount of feldspar. D = HJ19. One of the two samples in the study that contains poikilotopik calcite (white). E-G CL-images. E = CL7. Quartz cements are immeasurable due to feldspars in the view. F = HJ15. The sample shows small amounts of quartz cement in CL, white arrows points at the small amount. G = HJ13. Relief in thin-sections can be misinterpreted as quartz overgrowths.

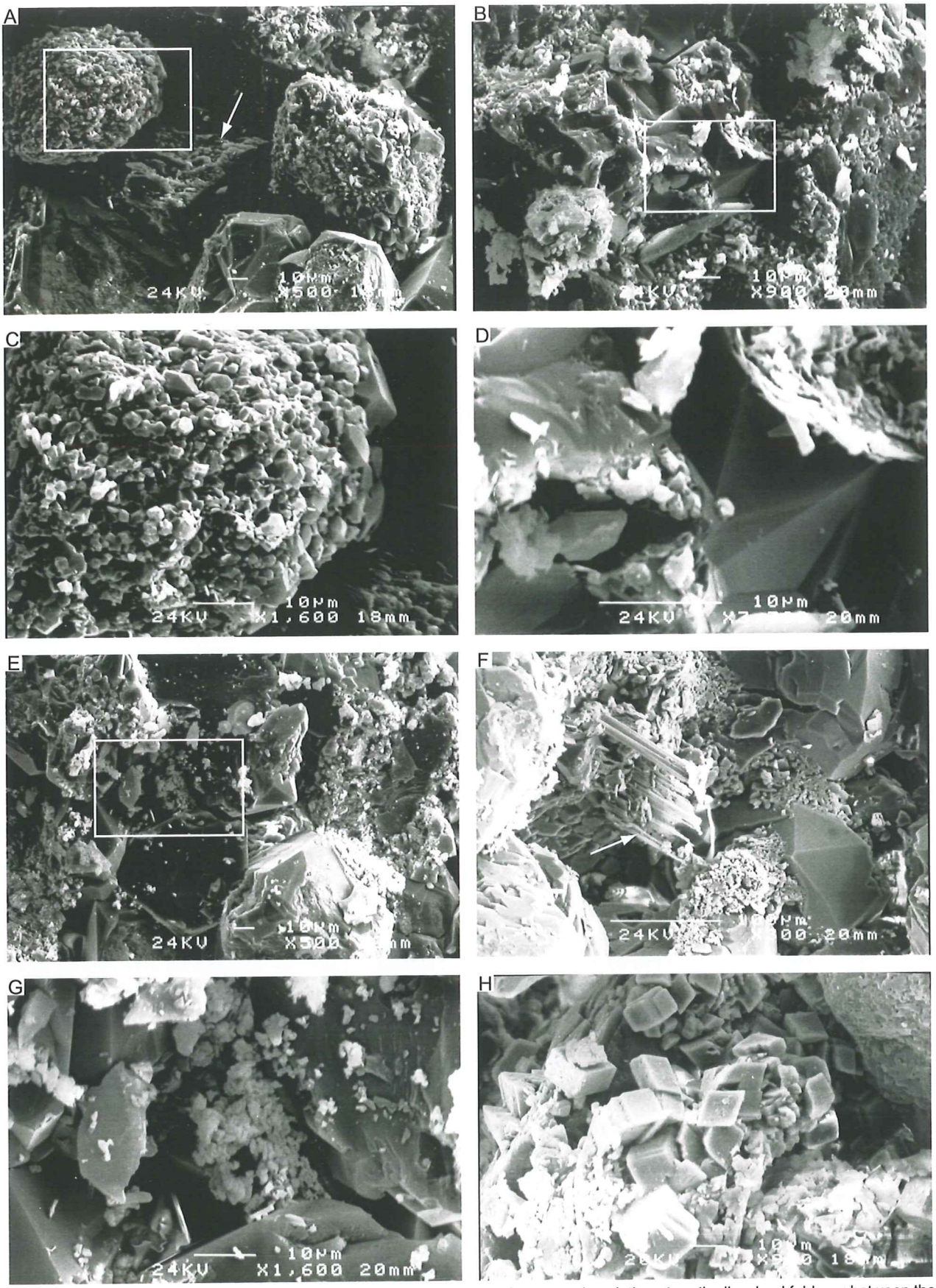

Fig. 12. Fig. 12. A,C = HJ10. The sample show micro quartz on two grains, arrow is pointing at partly dissolved feldspar between the two grains. B,D = HJ4. The slides show euhedral quartz overgrowths. E,G = HJ7 The slides show authigenic kaolinite. F = HJ16 Arrow is pointing at strongly weathered feldspar, a second diagenetic phase of authigenic kaolinite and quartz cement in form of micro quartz surrounds the feldspar. H = HJ14. Small amounts of authigenic carbonate in a high permeable sample.

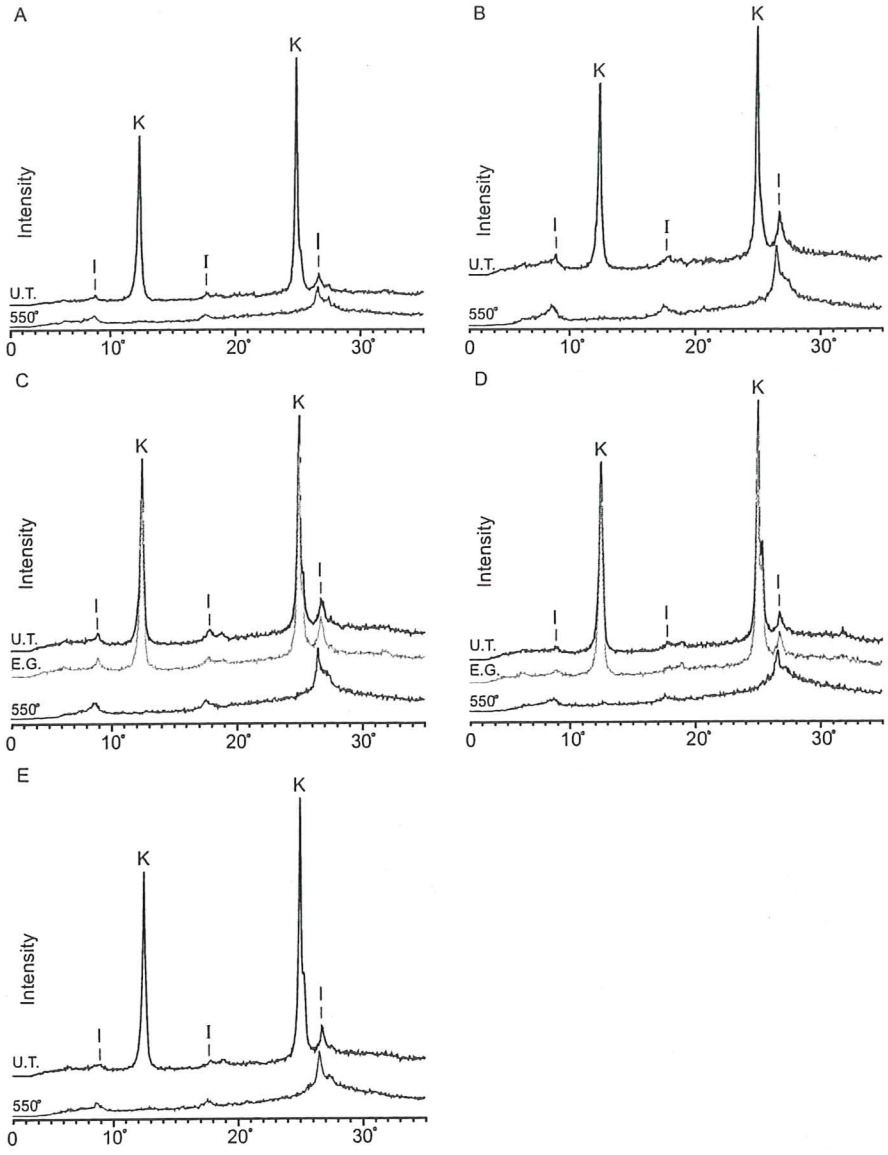

Fig. 13. XRD patterns of diagenetic clay, samples A-E. K=Kaolinite, I=Illite, U.T.=Untreated, 550º =Heated to 550º C, E.G.=Pretreated with ethylene glycol.

quently these have negligible permeability and porosity. Both samples have intergranular volumes comparable to the samples that lack calcite cementation. This implies that the calcite probably precipitated in the sandstone after compaction at maximum burial depth. According to Ahlberg (1994), calcite cements of the Helsingborg Member precipitated during burial diagenesis (<70°C). Probable ion sources for the siderite and calcite cements include dissolved molluscs, kerogen maturation and dissolution of plagioclase (Ahlberg 1994).

Quartz cementation is a common feature at different strata and is not bound to certain facies in the investigated drill cores. The more permeable arenites showed only small amounts of quartz cement and very little authigenic kaolinite, while the less permeable layers contains abundant quartz overgrowths and authigenic kaolinite. Sources for quartz cementation in sandstone may be derived internally from: (1) more soluble silica phases, e.g., amorphous silica (biogenic and volcanic) and opal CT, (2) dissolution of quartz, primarily by pressure solution and (3) mineral reactions involving the release of silica from dissolving silicate minerals (Bjørlykke & Egeberg, 1993). Affected silicate minerals such as feldspars are primarily observed in the less permeable beds, which have probably been subjected to meteoric flushing that caused the feldspar to dissolve (cf. Worden & Barclay 2000):

$$2KAlSi_3O_8 + 2H^+ + H_2O \rightarrow Al_2Si_2O_5(OH)_4 + 4SiO_2 + 2K^+$$

K-Feldspar Kaolinite Quartz

According to the formula the necessary ions for quartz cement and authigenic kaolinite can be derived from alteration of the feldspar, which is observed in most samples containing quartz cement and authigenic kaolinite (Fig 12a,f).

Sample HJ7 illustrates quartz overgrowths, authigenic kaolinite and strongly weathered feldspars, when examined in SEI. Examined in CL, sample HJ7 showed weathered feldspars, but no detectable quartz overgrowths. Sample HJ7 is collected from a sandstone lens in a succession encased in heteroliths and mudstones (Fig 4). Presumably the lens has been attached to other lenses, where fluids transported the necessary ions obtained from the sur-

rounding layers. This theory is also a reasonable explanation for the calcite cement in HJ5. Observations from SEI samples showed that in the surrounding environment of dissolved feldspar was a high proportion of quartz overgrowths and authigenic kaolinite, post-dating already established quartz cement (Fig 12f). This indicates that there have been either two diagenetic events or two different controlling factors that caused the quartz overgrowths.

However, combining the indication of quartz overgrowth with the anisotropy in the cores reveals further understanding for the diagenetic history. As mentioned before, mud matrix and mud drapes within the heteroliths and the mudstones in the cores is the strongest reducing factor for permeability and porosity, and is the major cause of anisotropy in the succession. Therefore, the flow is horizontally directed and blocked vertically. This would control both meteoric flushing effects and later diagenetic processes. However, in general this study shows that porosity and permeability reductions caused by diagenetic features is limited, compared to the depositional effects.

The heteroliths with its deltaic origin represent some of the strata in the North Sea that superimpose hydrocarbon-bearing units. The reservoir heterogeneity has for some time been known as a reducing factor for oil exploitation. In 1988 the first successful horizontal drilling, from a floating unit, was conducted in the North Sea (Brennand *et al.*, 1990). Recent trials with injecting sand or gas vertically, from a horizontal drilling, into the heteroliths, have provided a successful result in oil extraction. However, the anisotropy in reservoirs is not fully understood and is often, for convenience, mathematically modelled with assumed petrographical and petrophysical properties. Therefore, studies like this one are of vital importance in order to obtain valid determinations of reservoir characteristics.

Acknowledgements

I first wish to thank my supervisor Dr Anders Ahlberg Lund University, who has guided me through this thesis. Permeability and porosity measurements were carried out at the Institute for Environmental and Resources, Technical University of Denmark (DTU), where Dr Niek Molenar and Sinh Nguyen have been an immense help. Takhesi Miyazu is not forgotten for withstand my constant imposition. Thanks to Guy Bastin for being my adviser with the English language. I would also like to thank Professor Kent Larsson and Dr Sofie Lindström for critical comments on the manuscript. Pär Malmborg, for the assistance through long hours in the computer microlab. Last but with most love, I would like to thank Ulrika and Alma for their support and encouragement.

References

Ahlberg, A., 1994: Deposition and diagenesis of the Rhaetian-Hettangian succession (Triassic-Jurassic) in southern Sweden: preprints. *Lund publications in geology 123*, 1-53.

Ahlberg, A., Sivhed, U. & Erlström, M., 2001: The Jurassic of Southern Sweden. In: *The Jurassic of Denmark, Greenland and adjacent areas.* Editors: Surlyk F. & Ineson. Geology of Denmark Bulletine, 1-15, in press.

Bjørlykke, K., & Egeberg, P.K., 1993: Quartz cementation in sedimentary basins. *The American Association of Petroleum Geologists Bulletin 77(9)*, 1538-1548.

Brennand, T.P., Van Hoorn, B. & James, K.H., 1990: Historical review of North Sea Exploration. In: *Introduction to the Petroleum Geology of the North Sea*, 1-33. Editor: K. W. Glennie. Third edition. Blackwell Scientific Publications.

Budd, D. A., Hammes, U. & Ward, W. B., 2000: Cathodoluminescence in calcite cements: New insights on Pb and Zn sensitizing, Mn activation, and Fe quenching at low trace-element concentrations. *Journal of Sedimentary Research Section A: Sedimentary Petrology and Processes 70(1)*, 217-226.

Cooper, M. R., Evans, J., Flint, S. S., Hogg, A. J. C. & Hunter, R. H., 2000: Quantification of detrital, authigenic and porosity components of the Fontainebleau sandstone: a comparison of conventional optical and combined scanning electron microscope-based methods of modal analyses. In: *Quartz cementation in sandstones*, 89-101. Editors: R. H. Worden & S. Morad. Special Publication of the International Association of Sedimentologists 29.

Dott, R. H., 1964: Wacke, greywacke and matrix – What approach to immature sandstone classification?. *Journal of Sedimentary petrology 34*, 625-632.

Friedman, G. M., 1998: Rapidity of marine carbonate cementation - implications for carbonate diagenesis and sequence stratigraphy: perspective. *Sedimentary Geology* 119(1-2), 1-4.

Grigelis, A., & Norling, E., 1999: Jurassic geology and foraminiferal faunas in the NW part of the East European Platform. *Geological Survey of Sweden, Research Papers Ca 89*, 1-101.

Jahren, J., & Ramm, M., 2000: The porosity-preserving effects of microcrystalline quartz coatings in arenitic sandstones: examples from the Norwegian continental shelf. In: *Quartz cementation in sandstones*, 271-280. Editors: R. H. Worden & S. Morad. Special Publication of the International Association of Sedimentologists 29.

Miller, J. 1988: Cathodoluminescence microscopy. In: *Techniques in sedimentology*, 229-273. Editor: M. Tucker. Blackwell scientific publications, Oxford.

Morad S. 1998: Carbonate cementation in sandstone: distribution patterns and geochemical evolution. In: *Carbonate Cementation in Sandstones*, 1-26. Editor: S. Morad. Special Publication of the International Association of Sedimentologists 26.

Norling, E., Ahlberg, A., Erlström, M. & Sivhed, U., 1993: Guide to the Upper Triassic and Jurasssic geology of Sweden. *Geological Survey of Sweden, Research Papers Ca 82*, 1-71.

Norling, E., & Bergström, J., 1987: Mesozoic and Cenozoic tectonic evolution of Scania, southern Sweden. In: *Compressional Intra-Plate deformations in the Alpine Foreland,* 7-19. Editor: P.A. Ziegler. Tectonophysics 137 (1-4).

Owen, M. R., 1991: Application of Cathodoluminescence to sandstone provenance. In: *Luminescence microscopy and spectroscopy; qualitative and quantitative applications*, 67-75, 176-177. Editors: C. E. Barker & O. C. Kopp. SEPM short course notes 25.

Trewin, N., 1988: Use of the scanning electron microscope in sedimentology. In: *Techniques in sedimentology*, 229-273. Editor: M. Tucker. Blackwell scientific publications, Oxford.

Troedsson, G., 1950: On rhythmic sedimentation in the Rhaetic-Liassic beds of Sweden. *International Geological Congress Rep. XVIIIth session. 1948. Part 4, section C*, 64-72.

Troedsson, G., 1951: On the Höganäs series of Sweden (Rhaeto-Lias). *Lunds Universitets Årsskrift, N. F. 2,* 47(1), 269 pp.

Vossmerbäuer, H., 1970: Untersuchungen zur Bildungsgeschichte des Unteren Lias in Schonen (Schweden). *Geologica et Palaeontologica 4*, 167-193.

Worden, R. H, & Barclay, S. A., 2000: Internally sourced quartz cement due to external derived CO_2 in sub-arcosic sandstones, North Sea. *Journal of Geochemical exploration, 69-70,* 645-649.

Tidigare skrifter i serien "Examensarbeten i Geologi vid Lunds Universitet":

85. Strömberg, Caroline, 1997: The conodont genus *Ctenognathodus* in the Silurian of Gotland, Sweden.
86. Borgenlöv, Camilla, 1997: Vätskeinklusioner som ledtrådar till bildningsmiljön för Bölets manganmalm, Västergötland, södra Sverige.
87. Mårtensson, Thomas, 1997: En petrografisk och geokemisk undersökning av inneslutningar i Nordingrågraniten.
88. Gunnemyr, Lisa, 1997: Spårämnesförsök i konstgjort infiltrerat vatten - en geologisk och hydrogeologisk studie av Strömsholmsåsen, Hallstahammar, Västmanland.
89. Antonsson, Christina, 1997: Inventering, hydrologisk klassificering samt bedömning av hydrogeologisk påverkan av våtmarksområden i samband med järnvägstunnelbyggnation genom Hallandsåsen, NV Skåne.
90. Nordborg, Fredrik, 1997: Granens mark-påverkan - en studie av markkemi, jordmånsbildning och lermineralogi i gran- och lövskogsbestånd i södra Småland.
91. Dobos, Felicia, 1997: Pollen-stratigraphic position of the last Baltic Ice Lake drainage.
92. Nilsson, Johan, 1997: The Brennvinsfjorden Group of southern Botniahalvøya, Nordaust-landet, Svalbard - structure, stratigraphy and depositional environment.
93. Tagesson, Esbjörn, 1998: Hydrogeologisk studie av grundvattnets kloridhalter på östra Listerlandet, Blekinge.
94. Eriksson, Saskia, 1998: Morängenetiska undersökningar i klintar vid Greifswalder Boddens södra kust, NÖ Tyskland.
95. Lindgren, Johan, 1998: Early Campanian mosasaurs (Reptilia; Mosasauridae) from the Kristianstad Basin, southern Sweden.
96. Ahnesjö, Jonas, B., 1998: Lower Ordovician conodonts from Köpings klint, central Öland, and the feeding apparatuses of *Oistodus lanceolatus* Pander and *Acodus deltatus* Lindström.
97. Rehnström, Emma, 1998: Tectonic stratigraphy and structural geology of the Ålkatj-Tielma massif, northern Swedish Caledonides.
98. Modin, Anna-Karin, 1998: Distributionen av kadmium i moränmark kring St. Olof, SÖ Skåne.
99. Stockfors, Martin, 1998: High-resolution methods for study of carbonate rock: a tool for correlating the sedimentary record.
100. Zillén, Lovisa, 1998: Late Holocene dune activity at Sandhammaren, southern Sweden -chronology and the role of climate, vegetation, and human impact.
101. Bernhard, Maria, 1998: En paleoekologisk -paleohydrologisk undersökning av våtmarks-komplexet Rolands hav, Blekinge.
102. Carlemalm,Gunnar, 1999: En glacialgeologisk studie av morän och moränfyllda sprickor i underliggande sandursediment, Örsjö, Skåne.
103. Blomstrand, Malou, 1999: 1992-1998 Seismicity and Deformation at Mt. Eyjafjalla-jökull volcano,South Iceland.
104. Dahlqvist, Peter, 1999: A Lower Silurian (Llandoverian) halysitid fauna from the Berge Limestone Formation, Norderön, Jämtland, central Sweden.
105. Svensson, Magnus A., 1999: Phosphatized echinoderm remains from upper Lower Ordovician strata of northern Öland, Sweden - preservation, taxonomy and evolution.
106. Bengtsson, Anders, 1999: Trilobites and bradoriid arthropods from the Middle and Upper Cambrian at Gudhem in Västergötland, Sweden.
107. Persson, Christian, 1999: Silurian graptolites from Bohemia, Czech Republic.
108. Jacobson, Mattias, 1999: Five new cephalopod species from the Silurian of Gotland.
109. Augustsson, Carita, 1999: Lapillituff som bevis för underjurassisk vulkanism av strombolikaraktär i Skåne.
110. Jensen, Sigfinn J., 1999: En silurisk transgressiv karbonatlagerföljd vid S:t Olofsholms stenbrott, Gotland.
111. Lund, Mats G., 1999: En strukturgeologisk modell för berggrunden i Sarvesvagge - Luottalako-området, Sareks Nationalpark, Lappland.
112. Magnusson, Jakob, 1999: Exploration of sub-marine fans along the Coffee Soil Fault in the Danish Central Graben.
113. Wickström, Jenny, 1999: Conodont bio-stratigraphy in Volkhovian sediments from the Mäekalda section, north-central Estonia.
114. Sjögren, Per, 1999: Utmarkens vegetations-utveckling vid Ire i Blekinge, från forntid till nutid - en pollenanalytisk studie.
115. Sälgeback, Jenny, 1999: Trace fossils from the Permian of western Dronning Maud Land, Antarctica.
116. Söderlund, Pia, 1999: Från gabbro till granat-amfibolit. En studie av metamorfos i Åker-metabasiten väster om Protoginzonen, Småland.
117. Jönsson, Karl-Magnus, 2000: Sedimentologiska och litostratigrafiska undersökningar i södra Malmös kvartära avlagringar, södra Sverige.
118. Romberg, Ewa, 2000: En sediment- och

biostratigrafisk undersökning av den tidigare Littorina-lagunen vid Barsebäck, SV Skåne, med beskrivning av en Preboreal klimatoscillation.

119. Bergman, Jonas, 2000: Skogshistoria i Söderåsens nationalpark. En pollenanalytisk studie i Söderåsens nationalpark, Skåne.
120. Lindahl, Anna, 2000: En paleoekologisk och paleohydrologisk studie av fuktängar i Bräkneåns dalgång, Bräkne-Hoby, Blekinge.
121. Eneroth, Erik, 2000: En paleomagnetisk detaljstudie av Sarekgångsvärmen.
122. Terfelt, Fredrik, 2000: Upper Cambrian trilobite faunas and biostratigraphy at Kakeled on Kinnekulle, Västergötland, Sweden.
123. Sundberg, Sven Birger, 2000: Vattenrening genom komplexbildning mellan järn och humusämnen - en litteraturstudie med försök.
124. Sundberg, Sven Birger, 2000: Sedimentationsprocesser och avlagringsmiljö för en kantrygg kring platåleran vid Rydsgårds gods i backlandskapet söder om Romeleåsen, Skåne.
125. Kjöllerström, Anders, 2000: En geokemisk studie av bergartsvariationen på Bullberget i västra Dalarna.
126. Cinthio, Kajsa, 2000: Senglacial och tidigholocen etablering och expansion av lövträd på en lokal i nordvästra Rumänien.
127. Lamme, Sara, 2000: Klimat- och miljöförändringar under holocen i Sylarnaområdet, södra svenska Skanderna, baserat på analys av makrofossil och klyvöppningar.
128. Jönsson, Charlotte, 2000: Geologisk och hydrogeologisk modellering av området mellan Bjuv och Söderåsen, nordvästra Skåne.
129. Kleman, Johan, 2001: Utvärdering av den underkambriska litostratigrafin på Österlen, södra Sverige.
130. Sundler, Malin, 2001: En jämförande studie mellan uppmätt och MACRO-simulerad pesticidutlakning på ett odlingsfält i Skåne.
131. Grönholm, Anna, 2001: Högtrycksmetabasiter i den södra delen av Mylonitzonen: fältgeologi, petrografi och metamorf utveckling.
132. Ekdahl, Magnus, 2001: En studie av Källsjögranitens deformationsmönster och kinematiska indikatorer inom Ullaredszonen.
133. Axheimer, Niklas, 2001: Middle Cambrian trilobites and biostratigraphy of the Almbacken drill core, Scania, Sweden.
134. Lindén, Mattias, 2001: Proglacial deformation of glaciofluvial sediments during the Pomeranian deglaciation in the Neubrandenburg area, NE Germany.
135. Warnhag, Jon, 2001: A geochemical study of the zoned Pan-African Mon Repos intrusion, Central Namibia.
136. Lundmark, Mattias, 2001: Zirkonstudie av Norra Hortens bergarter, SV Sverige.
137. Gunnarson, Rebecka, 2001: Sedimentologisk undersökning av en moränskärning i en djupvittrad sprickdal på Romeleåsen, Skåne.
138. Karlsson, Christine, 2001: Diagenetic and petrophysical properties of deeply versus moderately buried Cambrian sandstones of the Caledonian foreland, southern Sweden.
139. Eriksson, Mårten, 2001: Bedömning av föroreningsspridning kring en nedlagd bensinstation i Karlaby, sydöstra Skåne.
140. Ljung, Karl, 2001: A paleoecological study of the Pleistocene-Holocene transition in the Kap Farvel area, South Greenland.
141. Åkesson, Cecilia, 2001: Undersökning av grundvattenförhållanden i området kring Östra Vemmerlöv, Simrishamns kommun, sydöstra Skåne.
142. Bermin, Jonas, 2001: Modelling Mössbauer spectra of biotite.
143. Mansurbeg, Howri, 2001: Modelling of reservoir quality in quartz-rich sandstones of the Lower Cretaceous Bentheim sandstones, Lower Saxony Basin, NW Germany.
144. Hermansson, Tobias, 2001: Sierggavággeskollans strukturgeologiska utveckling; nyckeln till Sareks berggrundsgeologi.
145. Veres, Daniel-Stefan, 2001: A comparative study between loss on ignition and total carbon analysis on Late Glacial sediments from Atteköps mosse, southwestern Sweden, and their tentative correlation with the GRIP event stratigraphy.
146. Ahlberg, Tomas, 2001: Hydrogeologisk undersökning samt sårbarhetskartering av området kring tre bergborrade grundvattenanläggningar i Simrishamns kommun.
147. Boman, Daniel, 2001: Tektonostratigrafi och deformationsrelaterad metamorfos i norra Kebnekaisefjällen, Skandinaviska Kaledoniderna.
148. Olsson, Stefan, 2002: The geology of the Portobello Peninsula; proposal of a saturated to oversaturated lineage within the Dunedin Volcano, New Zealand.
149. Molnos, Imre, 2002: Petrografi och diagenes i den underkambriska lagerföljden i Skrylle, Skåne.
150. Malmborg, Pär, 2002: Correlation between diagenesis and sedimentary facies of the Bentheim Sandstone, the Schoonebeek field, The Netherlands.
151. Jonsson, Henrik, 2002: Permeability variation in a tidal Jurassic deposit, Höganäs basin, Fennoscandian Border Zone